Optical Gain in the Near Infrared by Light-Emitting Electrospun Fibers

Giovanni Morello, Maria Moffa, Salvatore Girardo, Andrea Camposeo,* and Dario Pisignano**

The potential integration of polymer nanofibers in photonic devices and circuits is a major driver for research on their waveguiding and optical gain properties. Emission in the near-infrared is especially important in this framework in view of the realization of nanofiber-based optical amplifiers. Here, the optical gain properties of electrospun fibers embedding near-infrared light-emitting molecules are investigated. Upon pulsed optical pumping, line narrowing typical of amplified spontaneous emission is observed, with gain of 5.5 cm^{-1} and threshold fluence down to 0.25 mJ cm^{-2}. Importantly, the stimulated emission characteristics are strongly dependent on individual fiber characteristics and on the mutual alignment of nanofibers in arrays, thus being tailorable through the fiber architecture and assembling. These results open interesting perspectives for the exploitation of electrospun fibers as active components in the near-infrared range.

1. Introduction

The miniaturization of photonic and electro-optical devices is among the most fascinating challenges engaged by the scientific research in the last years. This is driven by the need of obtaining faster optical signal processing through more and more compact and flexible components, allowing for efficient generation and transmission of data.[1–3] To this aim, the design and the realization of a new generation of active and passive waveguides,[4–7] eventually based on fiber-shaped nanomaterials, are relevant goals. In particular, active waveguides are useful to facilitate coupling of incoming photons and to reduce optical losses.[5–7] In this framework, plastic optical fibers exhibit further advantages such as high mechanical flexibility, tailorable morpho-mechanical properties, and relatively low production cost. In addition, signal transmission in these fibers can be improved by doping them with suitable organic dyes or semiconductor nanoparticles,[5] spanning the spectral range from UV to near infrared (NIR).[8] NIR wavelengths are especially important, allowing these components to approach the main telecommunication windows.

Typically, polymer fibers are drawn from melts at high temperature, a process that can be strongly detrimental for the optical properties of embedded compounds, particularly for organic molecules. Polymer fibers can be also physically drawn from solutions,[6,9] allowing to obtain uniform fibers and well-preserving the emission features of active dopants. In this framework, electrospinning may represent a powerful, alternative method for realizing active, NIR-emitting polymer fibers by means of continuous production runs. This approach would combine relatively high throughput and low cost,[10] allowing miniaturization to be achieved, and preserving the optical and gain properties of embedded dopants, since entirely working at room temperature. Electrospun nanofibers have already shown interesting performances in terms of emission efficiency, waveguiding and laser action in the visible spectral range,[11] whereas there is still no report on NIR-gain features.

Here, we present electrospun fibers composed by an inert and optically-transparent polymer doped with fluorescent molecules, showing optical waveguiding and gain in the NIR with good performances (gain up to 5.5 cm^{-1}). Importantly, the stimulated emission is strongly dependent on the characteristics of the produced nanomaterial, particularly on the mutual alignment of fibers, which makes optical amplification controllable through fiber assembling. These results constitute the base for the exploitation of electrospun light-emitting fibers in photonic devices such as ultra-compact amplifiers and nanolasers operating in the NIR spectral range.

2. Results and Discussion

We electrospin a solution of poly(methylmetacrylate) (PMMA) doped with benzoxazolium, 2-[[2-[2-[4-(dimethylamino) phenyl]ethenyl]-6-methyl-4H-pyran-4-ylidene]methyl]-3-ethyl iodide (hereafter referred to as LDS 720) and 5-chloro-2-[2-[3-[(5-chloro-3-ethyl-2(3H)-benzothiazol- ylidene)ethylidene]-2-(diphenylamino)-1-cyclopenten-1-yl]ethenyl]-3-ethyl

Dr. G. Morello, Dr. M. Moffa, Dr. S. Girardo, Dr. A. Camposeo, Prof. D. Pisignano
National Nanotechnology Laboratory of Istituto Nanoscienze-CNR
via Arnesano, Lecce
73100, Italy
E-mail: giovanni.morello@nano.cnr.it; andrea.camposeo@nano.cnr.it; dario.pisignano@unisalento.it

Dr. G. Morello, Dr. A. Camposeo, Prof. D. Pisignano
Center for Biomolecular Nanotechnologies @ UNILE
Istituto Italiano di Tecnologia (IIT), Via Barsanti 1, Arnesano (LE)
73010, Italy

Prof. D. Pisignano
Dipartimento di Matematica e Fisica "Ennio De Giorgi"
Università del Salento
via Arnesano, Lecce
73100, Italy

DOI: 10.1002/adfm.201400395

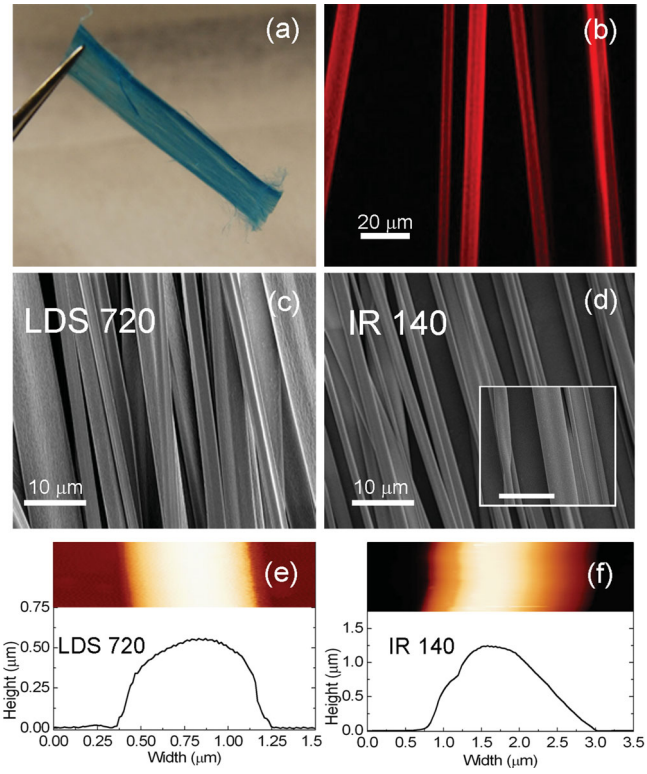

Figure 1. (a) Photograph of a free-standing array of uniaxially aligned LDS 720-based electrospun fibers. (b) Confocal micrograph of LDS 720-based fibers. (c,d) SEM micrographs of aligned fibers doped with LDS 720 and IR 140, respectively. Inset in (d): SEM image of twisted and folded fibers. Scale bar = 10 μm. (e,f) Exemplary AFM images and height profiles of LDS 720 and IR 140-based fibers, respectively.

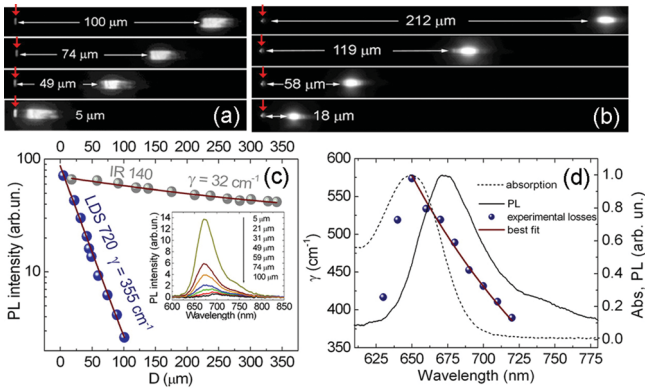

Figure 2. (a,b) Images of LDS 720 (a) and IR 140-based fibers (b), excited at variable distances from the tip. The vertical arrows indicate the tip from which the PL signal is collected after transmission along the fiber longitudinal axis. (c) Plot of the tip-emitted PL intensity from single fibers, as a function of the distance D (symbols) and relative best fits to equation, $I_{PL} = I_0 \cdot e^{-\gamma D}$ (lines). The estimated propagation losses are also shown. The data shown for LDS 720 are obtained in the range 700–740 nm. Inset: PL spectra collected from the tip of LDS 720-based fibers, at the various D values. (d) Plot of loss coefficient vs. wavelength, γ (left vertical scale). These data are obtained by fitting the intensity of the PL signal measured for various D at each wavelength, using an exponential decay curve (see text). The continuous line in (d) is a fit to the equation, $\gamma = C\,\lambda^{\beta}$. Absorption and emission spectra are also reported, as dotted and continuous lines, respectively (right vertical scale).

benzothiazolium perchlorate (IR 140, see Experimental Section). The resulting fibers are displayed in **Figure 1**. Macroscopic mats of both randomly oriented and uniaxially aligned fibers (Figure 1(a)) can be obtained by varying the electrospinning collection geometry. Confocal microscopy reveals the absence of appreciable clustering of dyes at the micrometer scale, which would be detrimental for both waveguiding and optical gain due to eventual increased scattering and local, concentration-induced fluorescence quenching. The embedded dyes are uniformly distributed along the length of each fiber. Indeed, individual fibers do not show any significant variation of their overall emission intensity in segments spaced by distances of the scale of many hundreds of μm, and through lengths of millimeters or more (Figure 1(b), and Figure S1 in Supporting Information). Differences in the signal intensity, collected from different points of the fiber bodies along their width as shown in Figure 1(b), are ascribed to partial or complete twisting and flattening of the fibers during deposition. Indeed, scanning electron microscopy (SEM) and atomic force microscopy (AFM) indicate that individual fibers are quite uniform along their longitudinal axis, defect-free, and generally exhibit a ribbon shape with an aspect ratio (fiber height:width) of about 1:2. Such shape favors the possible twisting and folding, as imaged in the inset of Figure 1(d). Ribbon-shape fibers are typically formed during electrospinning as a consequence of the collapse of a solid sheath formed on the surface of the liquid jet, due to the rapid evaporation of the solvent.[12] Importantly, there is no evidence of appreciable scattering centers such as break points and/or dye clustering.

We investigate the waveguiding properties of individual fibers by locally exciting them at variable distances (D) from their terminations, and collecting the photoluminescence (PL) signal emitted from the tips (**Figure 2**(a,b)). The optical excitation of the fiber body leads to PL emission, which is partially guided along the fiber up to the tip, from which light is then diffracted and out-coupled. This method so provides a clear insight into transmission performances, and into the origin of eventual optical losses.[13] The data of the PL intensity measured at the fiber tip, I_{PL}, are reported in Figure 2(c). A decrease of I_{PL}, as well as a significant red-shift of the detected signal is found upon increasing D (~25 nm for $D = 100$ μm in LDS 720 fibers, inset of Figure 2(c)). The intensity data can be well-fitted by the equation, $I_{PL} = I_0 \cdot e^{-\gamma D}$, where I_0 is a pre-exponential factor which indicates the intensity measured at very small D values, and γ is the loss coefficient. The fits lead to $\gamma = 355$ cm^{-1} for LDS 720 and $\gamma = 32$ cm^{-1} for IR 140-based fibers, respectively.

To rationalize the mechanisms affecting optical losses in the active waveguides, one has to take into account five main processes: self-absorption, Rayleigh scattering, surface-mediated losses, the possible evanescent coupling of light into the underlying substrate, and confinement effects.[13] Firstly, we notice that the significant spectral red-shift of PL, which we find for large D values, may be explained by the role played by self-absorption in affecting optical losses along fibers. Indeed, the largely different γ found in the two species of electrospun fibers can be attributed to the different Stokes shifts of the molecules, i.e. 65 meV and 124 meV for LDS 720 and IR 140, respectively (see Figure S2 in the Supporting Information), determining

different self-absorption of emitted light. Larger Stokes shifts of the dopants determine of course a reduced contribution of self-absorption to losses in the active waveguides. Following the method reported in Ref. [14] we quantify the role of self-absorption by calculating the ratio, S, of the absorption coefficients measured at the absorption and emission peaks. We find values of $S \cong 2$ and $S \cong 25$ for LDS 720 and IR 140, respectively. The ratio of these two values (about 12.5) is in good agreement with the ratio of the two γ coefficients obtained by the losses analysis (about 11.1), further confirming the prominent role of self-absorption in the here investigated systems.

Secondly, Rayleigh scattering considers the diffusion of light impinging on particles with dimension smaller than the wavelength. Though the exact contribution of this process to losses is not readily measurable, its influence can be unraveled by analyzing the behavior of the overall optical losses as a function of wavelength, since in media with Rayleigh scattering the intensity of transmitted light is proportional to λ^{-4}.[13] This analysis for LDS 720-based fibers is shown in Figure 2(d), where we plot the wavelength dependence of γ. By fitting the data to the expression, $\gamma = C\ \lambda^{\beta}$, a value of $\beta = -4.0 \pm 0.1$ is obtained in the range of wavelengths corresponding to PL emission. The strong deviations from this behavior which are observed at lower wavelengths are clearly attributable to the rapidly growing absorption as displayed in Figure 2(d). This suggests a non-trivial role of Rayleigh scattering at larger wavelengths where self-absorption decreases.

Other mechanisms play a minor role in this respect. Some light escapes laterally from the body of fibers due to surface-assisted scattering. These losses involve light propagating at angles larger than the critical one (strictly related to the orientation of the emitting dipoles inside the fiber), supported by surface roughness.[15] At angles larger than 30° with respect to the fiber longitudinal axis, this effect could lead to loss coefficients of several hundreds of cm^{-1}.[16] However, due to the absence of detectable signal along the fiber body nearby and far from the excitation point, we rule out this mechanism as possible major process contributing to the measured losses. Such a conclusion is in agreement with the morphological analysis performed on our electrospun fibers (Figure 1). In addition, we minimize evanescent coupling of light from the waveguides into the surrounding media by suspending the electrospun fibers in air.

Then, we study the optical gain properties of our fibers, deposited in uniaxially aligned arrays on quartz substrates and excited with a laser spot shaped in a stripe *parallel* to their alignment direction (see Experimental Section for details). For sake of comparison we also study reference films, spin-cast from the same solutions as those used for electrospinning. **Figure 3** displays the emission spectra of electrospun fibers and films with LDS 720, evidencing a clear spectral line-narrowing upon increasing excitation fluence, as typical of amplified spontaneous emission (ASE). Here ASE is peaked at about 735 nm, corresponding to the lower energy transition of LDS 720 (see insets of Figure 3(a,b)). ASE is observed at this wavelength since here the self-absorption of the active chromophores is 30 times smaller than that measured at the peak wavelength of the spontaneous emission (λ = 674 nm). Moreover, the lower energy transition makes the system equivalent to a four-level system,[17,18] which is known to be favorable for population inversion. The spectra undergo a rapid increase in intensity when the optical pumping exceeds a threshold, following

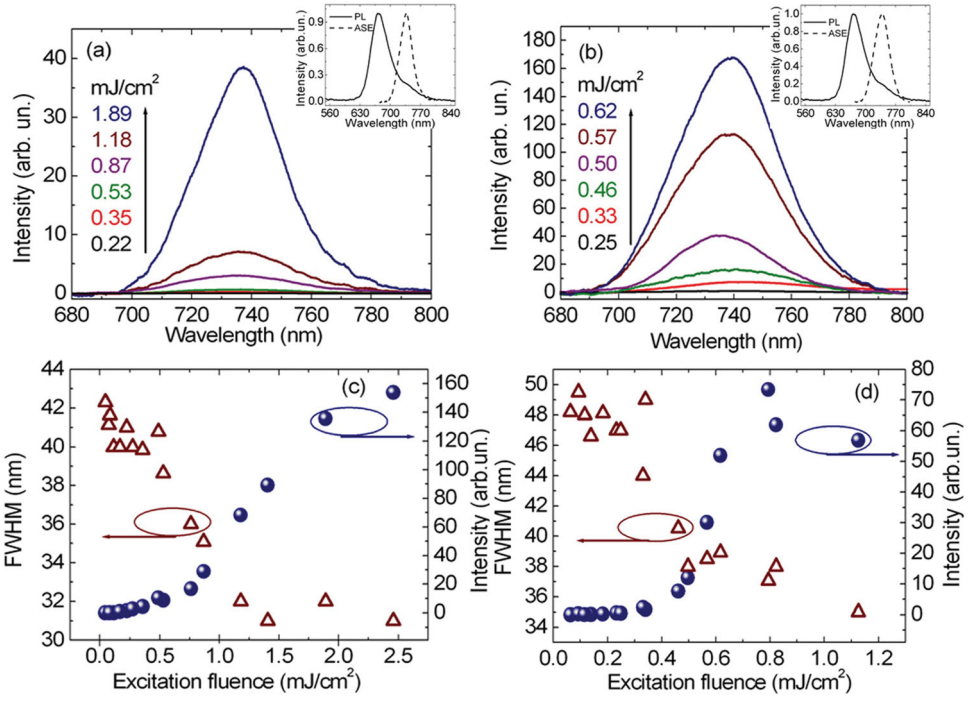

Figure 3. (a,b) ASE spectra of LDS 720-based fibers (a) and films (b), at various excitation fluences. The insets show the comparison between PL and ASE spectra. (c,d) Corresponding ASE intensity (full symbols) and FWHM of the emission spectra (empty symbols) as a function of the excitation fluence, for fibers (c) and films (d).

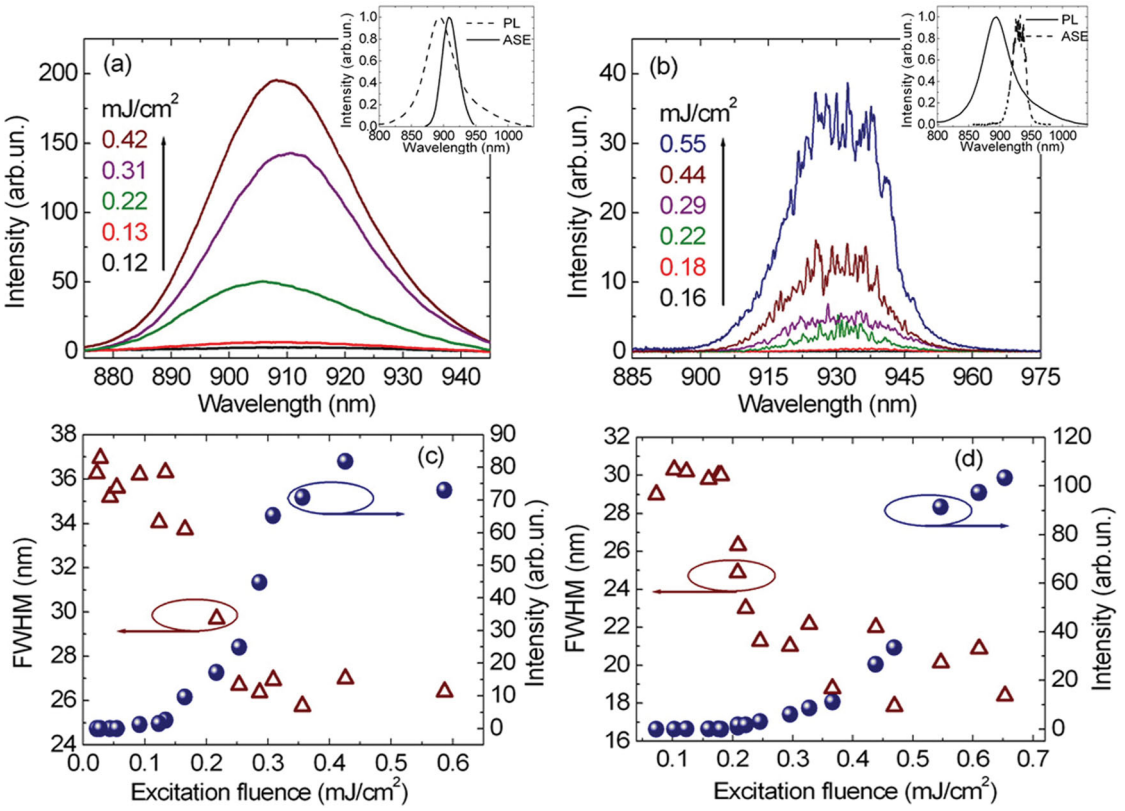

Figure 4. (a,b) ASE spectra of IR 140-based fibers (a) and films (b), at various excitation fluences. The insets show the comparison between PL and ASE spectra. (c,d) Corresponding ASE intensity (full symbols) and FWHM of the emission spectra (empty symbols) as a function of the excitation fluence, for fibers (c) and films (d).

a super-linear dependence (in the range 0.50–1.50 mJ/cm^2 for fibers and 0.45–0.80 mJ/cm^2 for films) until a saturation regime is reached (Figure 3(c,d)). This occurs when the amplification of the spontaneous emission reaches a value allowing the excited population to be significantly decreased, thus reducing the actual gain coefficient.[15] Concomitantly, the full width at half maximum (FWHM) of the emission spectra decreases as a consequence of the amplification, reaching a slightly lower value (~30 nm vs. 35 nm) for uniaxially aligned arrays of electrospun fibers. The found thresholds at about 0.45–0.50 mJ cm^{-2} are in accordance with values reported in the literature for dye-doped polymers.[19]

Figure 4 shows results of the same experiments on IR 140-based fibers and films. These materials exhibit some peculiarities, such as different ASE peak wavelengths for fibers and films, which can be attributed to the different conditions underwent by photons propagating in the two different geometries. In fact, the resulting film thickness (7.5 μm) is well above the cut-off condition for a planar waveguide (600 nm at $\lambda = 930$ nm). For fibers, we estimate a lower limit of about 1.4 μm for the microstructure thickness enabling effective waveguiding at 930 nm.[20] The estimated cut-off thickness is slightly larger than the measured fiber height (Figure 1(f)), which can induce a blue-shift of ASE as commonly observed in thin films.[21] The thickness-dependence of ASE from electrospun microstructures is also confirmed by the analysis of isolated fibers, for which we find that the emission peak wavelength varies depending on the specific excited fiber, with a minimum value of 880 nm attributable to the thinnest fibers (Figure S3 in the Supporting Information). Overall, this result indicates that in electrospun materials the gain emission peak can be finely tailored through the fiber structure and diameter.

By increasing the excitation density up to 0.3 mJ cm^{-2} the fiber ASE peak red-shifts by 4.5 nm, whereas a blue-shift (~1.5 nm) is observed for higher excitation densities (Figure 4(a)). As in other molecular systems,[22] the red-shift can be attributed to the increasing intensity of ASE (peaked at 906 nm) on the broad background of the spontaneous emission (peaked at 894 nm) following excitation increase, whereas the blue-shift at very high excitation intensities is to be ascribed to the competition between stimulated emission and energy relaxation upon photo-excitation of the active molecules.[22]

Moreover, the ASE spectra of IR 140-based films, but not those of fibers, show very sharp emission peaks (Figure 4(b)). The spectral position of these peaks changes with time and fluence, which are features typical of random lasers.[23] In our films, this effect can origin from light scattering by clusters of either the active molecules or the polymer matrix. In fact, imaging of the films under dark-field illumination (Figure S4) actually reveals the presence of clusters of various dimensions, from diffraction-limited size (<1 μm) to several micrometers. Interestingly, these scattering centers as well as the featured ASE spectra are not found in electrospun fibers

(Figure 1 and S1), which has to be related to the different processing conditions.

Being the observed random lasing a coherent process superimposed to the ASE, it somehow influences the figures of merit determined for the optical gain in the films.[24] First, the effective threshold is likely over-estimated, since the presence of coherent lasing deprives the potential population inversion for incoherent ASE. Second, the overall spectral broadening is reduced due to a major concentration of the optical modes around the lasing emission wavelengths. The measured thresholds for optical amplification are of about 0.30 mJ/cm^2 for films, and of about 0.25 mJ/cm^2 for electrospun fibers, and the FWHM undergoes a noticeable decrease from films to fibers (about one half). Hence, in this system moving from films to electrospun fibers significantly reduces the ASE threshold and linewidth, i.e. the nano/micrometer scale elongation of polymer macromolecules upon electrospinning suppresses the presence of NIR-light scattering centers. Finally it is worth to note that ASE is not observed by exciting with a stripe perpendicular to the alignment direction of fibers in the array, evidencing that optimal excitation conditions are achieved only by an excitation stripe extending parallel to the fiber longitudinal axis. This is also supported by the observation of a dependence of the excitation threshold on the degree of mutual alignment of the fiber axes, namely on the degree of mutual order of the organic filaments in the array. In particular, a higher threshold (about 2 mJ cm^{-2}) is found for randomly oriented fibers (Figure S5 of Supporting Information). These findings emphasize the fundamental role of waveguiding in determining the optical gain properties of the NIR-emitting electrospun fibers.

In **Figure 5**(a,b) we show the net gain spectrum as obtained by the variable stripe method.[15] In the waveguide, the output intensity I_L depends on the effective net gain, G_{eff}, and on the stripe length, L, as follows:

$$I_L = \frac{I_p A(\lambda)}{G_{eff}} \cdot [e^{G_{eff}(\lambda) \cdot L} - 1], \quad (1)$$

where I_p is the non-amplified PL intensity and $A(\lambda)$ depends on the cross section for spontaneous emission. The effective gain is in turn related to the stimulated emission gain by $G_{eff} = G_{se} - \gamma$, where $G_{se} = \sigma_{se} \cdot N_{exc}$, σ_{se} being the stimulated emission cross-section and N_{exc} representing the excited volume density. Finally, the stimulated emission cross-section can be expressed as:

$$\sigma_{se} = \frac{\lambda^4 \cdot f(\lambda)}{8\pi \cdot n^2 \cdot c\tau} \quad (2)$$

where $f(\lambda)$ is the normalized spectral distribution, c is the light speed in vacuum, n is the refractive index and τ is the radiative lifetime of the optical transition. Equation (2) leads to a G_{eff} behavior with a rapid increase upon increasing wavelength until the ASE peak [where $f(\lambda)$ is maximum] is reached and a possibly smoother, subsequent decay at longer wavelengths, as found experimentally (Figure 5). The extracted values of maximum gain (**Table 1**) are comparable to those reported in the literature for similar organic or nanocomposite systems in the visible spectral range.[15,25]

A maximum gain of 5.5 cm^{-1} and 4.2 cm^{-1} is found in LDS 720-based and IR 140-based fibers, respectively, making them suitable systems for the potential implementation of nanolaser sources and optical amplifiers assisted by the fiber waveguiding properties.[3,17,26,27] These values have to be related to the local excitation conditions and orientation of transition dipoles in the different electrospun materials. The unveiling of the ultimate mechanisms determining the optical gain will involve the assessment of the dopant radial distribution and of the supramolecular organization within electrospun nanofibers, which generally exhibit a complex and spatially-varying internal microstructure.[28,29]

Finally, we re-analyse the propagation losses in the gain spectral region and under pulsed excitation conditions, by measuring the PL intensity as a function of the distance (D) of the excitation stripe from the sample edge (Figure 5(c,d) and Table 1).[15] Interestingly, optical losses measured by ASE experiments (7 cm^{-1} and 11 cm^{-1} in LDS 720-based and IR 140-based fibers, respectively) are noticeably lower than those at the characteristic spontaneous emission wavelengths. In particular, at ASE wavelengths the contribution of self-absorption as source of losses is significantly reduced, due to the red-shift of ASE compared to spontaneous emission (insets of Figure 3(a,b) and 4(a,b)). These findings are rationalized by comparing the values of the S parameter calculated at the maximum PL wavelength (S_{PL}) with those calculated at the ASE peak wavelength (S_{ASE}). In LDS 720-based fibers, S_{ASE} is more than 30 times higher than S_{PL} ($S_{PL}/S_{ASE} \cong 3 \times 10^{-2}$) whereas in IR 140-based fibers S_{PL}/S_{ASE} is about 0.3, consistent with the differences arising in the losses determined from waveguiding (Figure 2(c)) and from ASE experiments (Table 1). These results, further highlighting the importance of self-absorption in the NIR-emitting electrospun

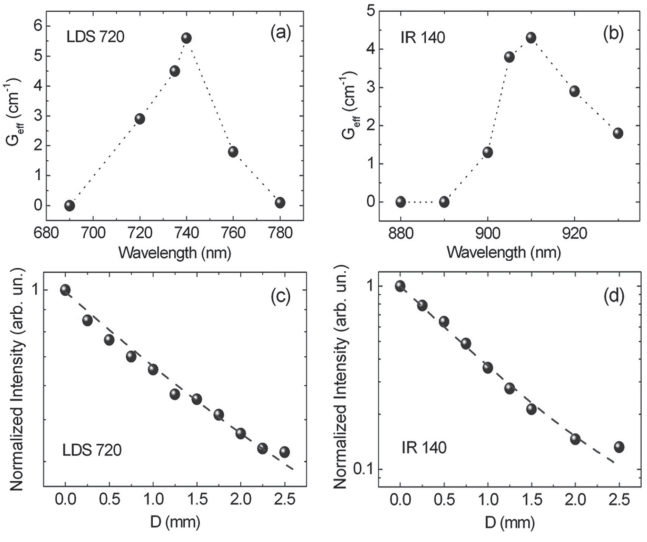

Figure 5. (a,b) Net gain of fibers (symbols) as a function of the emission wavelength. G_{eff} is determined by fitting the PL intensity vs. stripe length at each wavelength to Equation (1). Excitation fluence = 1.5 mJ/cm^2 (a) and 0.3 mJ/cm^2 (b). Dotted lines are guides for the eye. (c,d) Analysis of losses. Experimental values of the ASE intensity (symbols) are plotted vs. the distance of the exciting stripe from the emitting edge of the substrate. Excitation fluence = 1.5 mJ/cm^2 (c) and 0.3 mJ/cm^2 (d). Fitting lines are by equation: $I_{PL} = I_0 \cdot e^{-\gamma D}$ (dotted lines).

Table 1. Summary of the main optical and gain properties of LDS 720-based and IR 140-based spin-cast films and electrospun fibers.

Active Molecule	ASE peak wavelength (film/fibers) [nm]	ASE excitation threshold (film/fibers) [μJ/cm^2]	Maximum gain of fibers [cm^{-1}]	Losses of fibers [cm^{-1}]
LDS 720	735/735	450/500	5.5	7
IR 140	930/880-920	300/250	4.2	11

fibers, suggest doping by energy donor-acceptor molecular systems, with reduced spectral overlap between absorption and emission spectra, as next promising strategy to reduce optical losses.

3. Conclusions

We have demonstrated for the first time optical gain properties in the NIR spectral range in light-emitting electrospun fibers. Waveguiding has been also investigated, having insight into the prominent role of self-absorption and Rayleigh scattering on optical losses from the fibers. Electrospun fibers show reproducible thresholds for ASE (0.25–0.50 mJ cm^{-2}) and optical losses of 7–11 cm^{-1}, and good net gain values (up to 5.5 cm^{-1}), and waveguiding also plays a role in assisting ASE as evidenced by the strong dependence of the achievable gain on the architecture and alignment of fibers and of their ensembles. Noteworthy, the production of fibers results in removal of light scattering from molecular clusters. These results are very promising in view of the realization of fiber-based photonic devices and sensing elements operating in the NIR spectral range.

4. Experimental Section

Fiber Fabrication: Solutions for electrospinning are prepared dissolving PMMA (375 mg/mL) with either LDS 720 (0.62 mg/mL) or IR 140 (1.87 mg/mL) in chloroform, and placed under sonication at 40 °C for 6 hours. Both the solution concentrations and the PMMA/dye relative content are optimized in order to obtain uniform fibers with good net gain. In particular, the relative content of the dopants is crucial for gain, the latter being disfavored by the possible aggregation of the active molecules and at too high dye concentrations.[30–32] The solutions are then loaded into a 1 mL syringe and delivered at a constant flow rate (1 mL/h) through a metal needle (27 gauge) connected to a high-voltage power supply (EL60R0.6–22, Glassman High Voltage, High Bridge, NJ). Upon applying high voltage (10 kV), a fine polymer solution jet is ejected from the needle and deposited on 1 cm^2 quartz substrates. Uniaxially aligned arrays are obtained by collecting the fibers with a rotating disk (8 cm diameter, 1 cm thickness, 4000 rpm).

Morphological Characterization: The morphology of the fibers is investigated using SEM (Nova NanoSEM 450, FEI) after thermal deposition of 5 nm of Cr. The average width of fibers (3 μm for LDS 720-based fibers and 2 μm for IR 140-based fibers, respectively) is calculated from SEM micrographs analyzing a total number of at least 100 fibers. AFM is performed by a Multimode system equipped with a Nanoscope IIIa electronic controller (Veeco Instruments), operating in Tapping mode and using Si cantilevers with a resonance frequency of 250 kHz.

Absorption, PL and Confocal Measurements: Absorption measurements are performed on spin-cast films by a spectrophotometer (Varian Cary 300 Scan). PL spectra are recorded by exciting the films at λ_{exc} = 408 nm and analyzing the signal by a charge coupled device (CCD) camera (Jobin Yvon, Symphony). Confocal images (Olympus FV-1000) are collected by laser scanning (λ_{exc} = 405 nm) a random field of fibers, in epilayer configuration. The exciting laser is passed through an objective lens (40× and numerical aperture, N.A. = 0.75, resolving power ~550 nm), the PL is collected by the same objective and then analyzed by a multianode photomultiplier.

Waveguiding Measurements: Samples of fibers aligned on a quartz substrate are positioned on an inverted microscope. The fibers near the edge of the substrate are cut, thus being suspended from one end, resulting in a number of fibers protruding from the edge of the substrate by about 1 mm. A laser light (λ_{exc} = 408 nm) passing through an objective lens (20×, N.A. = 0.5) excites the fibers, whose emission is collected by the same objective, dispersed by a 0.33 m long monochromator and detected by a CCD, or alternatively directly sent to another CCD camera (Leica, DFC 490) without spectral dispersion, for imaging. An accurate tilting system allows the excitation spot to be translated along the fibers without optical distortions. The fibers are irradiated on their body at a measurable distance from the freestanding tip. For each position, we study the PL intensity from the fiber tip versus the distance, normalizing the data to the PL intensity collected from the excitation spot in order to account for local variations of the sample excitation, due to the positioning of the laser beam and eventual fluctuations of the excitation intensity (Figure 2(a,b)).

Optical Gain Characterization: Samples of films and aligned fibers are put under vacuum in order to prevent photoinduced degradation, and excited by the third harmonic of a pulsed Nd:YAG laser (λ_{exc} = 355 nm, repetition rate = 10 Hz, pulse duration = 10 ns). The experiments are performed in a side-pump configuration. The excitation spot is focused on the samples (parallel to the fibers alignment axis) in a stripe shape (maximum length = 4 mm, width = 150 μm), and with an end precisely positioned on one edge of the samples by means of a micrometric translation stage. The signal is collected from the edge. For ASE measurements, the stripe is focused on the sample keeping one end on the border of the substrate, and varying the excitation fluence. The sample signal, collected from the excited edge of the samples by means of a spherical lens (f = 75 mm), is coupled in a fiber-coupled monochromator and measured by a CCD. For net gain characterization the stripe length is varied by means of a slit, keeping fixed the excitation fluence at a value between the threshold and the saturation value. Optical losses are investigated by varying the distance of the 4 mm long stripe from the edge of the sample, at fixed fluence.

Acknowledgements

The authors acknowledge Dr. Pompilio Del Carro for help in morphological characterization. The financial support from the Italian Minister of University and Research FIRB RBFR08DJZI "Futuro in Ricerca" and the Apulia Regional Network of Public Research Laboratories No. 09 (WAFITECH) and No. 13 (M.I.T.T.) are also acknowledged.

Received: February 5, 2014
Revised: April 11, 2014
Published online: June 23, 2014

[1] A. Politi, M. J. Cryan, J. G. Rarity, S. Yu, J. L. O'Brien, *Science* **2008**, *320*, 646.
[2] D. Amarasinghe, A. Ruseckas, A. E. Vasdekis, G. A. Turnbull, I. D. W. Samuel, *Adv. Mat.* **2009**, *21*, 107.

[3] J. Clark, G. Lanzani, *Nat. Phot.* **2010**, *4*, 438.
[4] K. Srinivasan, O. Painter, *Nature* **2007**, *450*, 862.
[5] H. Liu, J. B. Edel, L. M. Bellan, H. G. Craighead, *Small* **2006**, *2*, 495.
[6] V. D. Ta, R. Chen, L. Ma, Y. J. Ying, H. D. Sun, *Laser Phot. Rev.* **2013**, *1*, 133.
[7] J. Wang, F. Chen, R. Li, H. Dong, J. Fan, L. Zhang, L. Shi, K. Y. Wong, *Appl. Phys. B* **2012**, *107*, 163.
[8] A. Camposeo, F. Di Benedetto, R. Stabile, R. Cingolani, D. Pisignano, *Appl. Phys. Lett.* **2007**, *90*, 143115.
[9] C. Meng, Y. Xiao, P. Wang, L. Zhang, Y. Liu, L. Tong, *Adv. Mater.* **2011**, *23*, 3770.
[10] L. Persano, A. Camposeo, C. Tekmen, D. Pisignano, *Macromol. Mater. Eng.* **2013**, *298*, 504.
[11] A. Camposeo, L. Persano, D. Pisignano, *Macromol. Mater. Eng.* **2013**, *298*, 487.
[12] S. Koombhongse, W. Liu, D. H. Reneker, *J. Polym. Sci. Pol. Phys.* **2001**, *39*, 2598.
[13] D. O'Carroll, I. Lieberwirth, G. Redmond, *Small* **2007**, *3*, 1178.
[14] M. J. Currie, J. K. Mapel, T. D. Heidel, S. Goffri, M A. Baldo, *Science* **2008**, *321*, 226.
[15] M. D. McGehee, R. Gupta, S. Veenstra, E. K. Miller, M. A. Dìaz-Garcia, A. J. Heeger, *Phys. Rev. B* **1998**, *58*, 7035.
[16] P. K. Tien, *Appl. Opt.* **1971**, *10*, 2395.
[17] I. D. W. Samuel, G. A. Turnbull, *Chem. Rev.* **2007**, *107*, 1272.
[18] O. Svelto, in *Principles of Lasers*, 4th ed., Springer, New York, USA **1998**, Ch. 1.
[19] A. J. Das, C. Lafargue, M. Lebental, J. Zyss, K. S. Narayan, *Appl. Phys. Lett.* **2011**, *99*, 263303.
[20] X. Song, R. Leonhardt, *Prog. Electromagn. Res.* **2013**, *135*, 81.
[21] A. K. Sheridan, G. A. Turnbull, A. N. Safonov, I. D. W. Samuel, *Phys. Rev. B* **2000**, *62*, R11929.
[22] D. Pisignano, M. Anni, G. Gigli, R. Cingolani, M. Zavelani-Rossi, G. Lanzani, G. Barbarella, L. Favaretto, *Appl. Phys. Lett.* **2002**, *81*, 3534.
[23] D. S. Wiersma, *Nat. Phys.* **2008**, *4*, 359.
[24] F. Quochi, *J. Opt.* **2010**, *12*, 024003.
[25] R. Zhang, H. Yu, B. Li, *Nanoscale* **2012**, *4*, 5856.
[26] J. R. Lawrence, G. A. Turnbull, I. D. W. Samuel, *Appl. Phys. Lett.* **2002**, *80*, 3036–3038.
[27] G. Heliotis, D. D. C. Bradley, M. Goossens, S. Richardson, G. A. Turnbull, I. D. W. Samuel, *Appl. Phys. Lett.* **2004**, *85*, 6122.
[28] I. Greenfeld, K. Fezzaa, M. H. Rafailovich, E. Zussman, *Macromolecules* **2012**, *45*, 3616.
[29] A. Camposeo, I. Greenfeld, F. Tantussi, S. Pagliara, M. Moffa, F. Fuso, M. Allegrini, E. Zussman, D. Pisignano, *Nano Lett.* **2013**, *13*, 5056.
[30] A. Mahfoud, A. Sarangan, T. R. Nelson, E. A. Blubaugh, *J. Lumin.* **2006**, *118*, 123.
[31] M. Fakis, I. Polyzos, G. Tsigaridas, V. Giannetas, P. Persephonis, I. Spiliopulos, J. Mikroyannidis, *Phys. Rev. B* **2002**, *65*, 195203.
[32] Z. E. Lampert, C. L. Reynolds Jr., J. M. Papanikolas, M. O. Aboelfotoh, *J. Phys. Chem. B* **2012**, *116*, 12835.